An Experimentally Validated Evaporative Phase Change Heat Transfer Model for Low Mass Flux Applications using R134a in Plate Heat Exchangers

John R. Simon III, Todd M. Bandhauer*

REACH CoLab, Colorado State University, Fort Collins, CO 80524, USA

*email: tband@colostate.edu
phone: 970-491-7357
fax: 970-491-3827
Address:
Colorado State University
Department of Mechanical Engineering
1374 Campus Delivery
Fort Collins, CO 80523

KEYWORDS: Plate frame heat exchangers, industrial refrigeration, heat transfer

NOMENCLATURE

A	area, m^2
C	heat capacity rate, kW K^{-1}
C_1	Wilson plot constant 1
C_2	Wilson plot constant 2
C_r	ratio of heat capacity rates
Co	confinement number
C_p	constant pressure specific heat, kJ kg^{-1} K^{-1}
CV	number of control volumes in a phase region
D_h	hydraulic diameter, m
G	mass flux, kg m^{-2} s^{-1}
h	heat transfer coefficient, kW m^{-2} K^{-1}
i	enthalpy, kJ kg^{-1}
j	vertical coordinate
k	thermal conductivity, kW m^{-1} K^{-1}
L	plate length, m
$\dot{m}$	mass flow rate, kg s^{-1}
N	Wilson plot velocity exponent
NTU	number of transfer units
Pr	Prandtl number
q	heat transfer rate, kW
q”	heat flux, kW m^{-2}
R	thermal resistance, m^2 K kW^{-1}
Re	Reynolds number
S	uncertainty of a parameter
T	temperature, ^{o}C
UA	overall conductance, kW K^{-1}
$\bar{V}$	velocity, m s^{-1}
W	plate width, m
Greek Symbols:	
β	chevron angle, ^{o}
δ	thickness, m
∂	uncertainty parameter value
ε	heat exchanger effectiveness
Subscripts:	
conv	convection
g	water-glycol
in	in
max	maximum
min	minimum
ov	overall
out	out
p	plate
r	refrigerant

sat	saturation
wall	wall
x	uncertainty input parameter
y	uncertainty parameter of interest

ABSTRACT

Plate frame heat exchangers are common in liquid-coupled vapor compression systems due to their compactness and ease of maintenance. In some of these systems, the refrigerant within the evaporator can enter the heat exchanger as a subcooled liquid. As a result, the refrigerant passes through three different phases: single-phase liquid, two-phase fluid, and a superheated vapor. Unfortunately, there have been limited prior studies that have identified the best method to predict performance under these circumstances. Furthermore, previous investigations have not evaluated refrigerant evaporation in large industrial sized plate frame heat exchangers under conditions experienced in the present study experimental test facility, especially at mass fluxes below 7 kg m^{-2} s^{-1}. In the present investigation, a model was developed to predict the performance of plate and frame heat exchangers when the fluid enters as a subcooled liquid and exits as a superheated vapor. The model used full-sized plate heat exchanger geometry that was discretized into 20 sections to accurately capture local heat transfer and pressure drop effects. The model was validated using an R134a counter flow heat exchanger used in a turbo-compression cooling system test facility that had subcooled liquid entering the evaporator at low mass fluxes. A variety of empirical correlations were evaluated to determine what combination yielded the best predictive capability over the following range of conditions: $5.8 < G < 6.8$ kg m^{-2} s^{-1}, $2 < q'' < 2.8$ kW m^{-2}, and $10°C < T_{sat} < 15°C$. When the correlations used a fixed control volume length in the heat flux calculation, the most accurate combination resulted in a mean absolute error of 5.5%. Future studies can use the approach described here to optimize heat exchanger size and performance.

1. INTRODUCTION

The evaporator is a critical component in thermal energy systems, including vapor compression cycles. In large commercial and industrial scale systems, liquid coupled evaporators are typically a shell and tube construction and the design process for these heat exchangers is well known [1–5]. Unfortunately, shell and tube heat exchangers have lower surface area to volume ratios, typically less than 100 m^2 m^{-3}, compared to compact plate frame heat exchangers which can have surface area to volume ratios between 120 to 660 m^2 m^{-3} [6]. Many heat transfer and pressure drop correlations for single-phase [7–14] and two-phase [15–24] fluids have been developed for plate frame heat exchangers that cover a range of geometries, operating parameters, and fluids. However, there have been limited studies that predict the performance or size of a plate frame heat exchanger in systems where the fluid enters as a single-phase, subcooled liquid and exits as a superheated vapor. In addition, many of these studies experimentally validated the heat transfer coefficients using small brazed plate type heat exchangers with very few plates and fluid flow channels, which are not indicative of all applications. Heat exchangers used in industrial applications can be significantly larger and contain hundreds of plates [25].

Though it is common for evaporators in vapor compression cycles to be designed with refrigerant entering as a two-phase fluid, some processes may require the evaporator to accept a subcooled refrigerant, especially during off design conditions. For example, vapor compression systems with a suction line heat exchanger (SLHX) use the evaporator discharge to pre-cool the fluid at the condenser outlet before it is expanded [26]. If the evaporator discharge is sufficiently cold, and the SLHX has a high effectiveness, it is possible that the fluid at the expansion valve inlet has a lower enthalpy than the evaporator saturated liquid enthalpy, thus causing the evaporator inlet to be a single-phase liquid. In addition, the working fluid typically enters the boiler of an organic Rankine cycle (ORC) as a subcooled liquid, and then exits as a superheated vapor before entering the turbine [27]. In both circumstances, it may be advantageous to have a single plate frame device. To assist in the design of these systems, there is a need for a model to accurately predict size and performance of an evaporator that can account for all fluid phases: from entering subcooled refrigerant, evaporating, to leaving as a superheated vapor.

Unfortunately, no prior studies were found which can predict performance of an evaporative heat exchanger including three fluid phase regions at low mass fluxes (5.8 - 6.8 kg m^{-2} s^{-1}) and low saturation temperatures (10°C-15°C) using a standard working fluid for industrial vapor compression systems. Eldeeb et al. [28] and Amalfi et al. [29] have compiled several empirical flow boiling heat transfer and pressure drop correlations for plate heat exchangers which may be appropriate for the two-phase region of the evaporator used in this study. In addition, some studies modify existing correlations to expand the range of validated operational conditions [30-31]. However, these correlations are only meant to provide the heat transfer coefficient for the refrigerant two-phase fluid region and do not address the heat transfer characteristics of the single-phase refrigerant or water-side flows. Longo et al. [32] extended this work by developing a method to account for boiler superheating by using a weighted average heat transfer coefficient which was computed as the average value between boiling and superheating zones of the heat exchanger. Lee et al. [33] conducted an experimental study which compared collected data to correlations from literature and found that Han et al. [15] had the closest agreement to experimental heat transfer coefficient. However, this study only focused on comparing correlations in the two-phase region and the test matrix included extremely low mass fluxes (1.28 to 1.7 kg m^{-2} s^{-1}) and higher saturation temperatures (18°C to 26°C) than those used in this study. A study by Jeong et al. [34] was the most similar to the present study and experimentally investigated correlations for use in a plate frame heat exchanger model for the evaporator of an ORC. The study was conducted using R245fa, saturation temperatures of 80°C to 90°C, and mass fluxes of 10.75 to 12.88 kg m^{-2} s^{-1}. The refrigerant saturation temperature in the Jeong et al. study [34] was high compared to saturation temperatures in vapor compression evaporators. For the water-side heat transfer coefficient, Jeong et al. [34] developed new empirical correlations because no correlation from literature agreed with experimental data. In addition, the refrigerant always entered the heat exchanger as a subcooled liquid but would sometimes exit as a two-phase mixture and an energy balance was used to calculate the fluids exit vapor quality.

The present study aims to develop a heat exchanger model that predicts evaporator performance or length of a plate frame heat exchanger where the refrigerant enters as a subcooled liquid and exits as a superheated vapor. The range of operating conditions were determined to be those typical in a turbo-compression cooling system [27] which used R134a with mass fluxes less than 7 kg m^{-2} s^{-1}, saturation temperatures less than 15°C, and heat fluxes less than 3 kW m^{-2}. In addition, the model was developed using an industrial sized plate heat exchanger which has a length greater than 1 m and had 300 heat transfer plates. This paper begins with a review of correlations for various flow regimes in plate frame heat exchangers which partially encompass some of the parameters investigated in this experimental study. Next, the experimental facility is described, including the characteristics of the plate frame heat exchanger studied here. Then, the modeling approach for the heat exchanger is described in detail. Finally, the correlations implemented into the model are compared with experimental results to determine the best combination that ensures accurate predictions.

2. SURVEY OF HEAT EXCHANGER CORRELATIONS

As described in the experimental setup below, the present investigation used 70-30 by volume water-propylene glycol mixture as the hot side working fluid and R134a as the cold side working fluid. The plate frame heat exchanger contained 150 fluid channels per side, or 300 total plates, that were 1.2 m long and 0.43 m wide. The hydraulic diameter of each channel was 5.1 mm with a 60° chevron angle. Operating conditions included mass fluxes 5.8 to 6.8 kg m^{-2} s^{-1}, heat fluxes 2 to 2.8 kW m^{-2}, and saturation temperatures 10 to 15°C (415 to 490 kPa). To determine the heat transfer coefficients for the refrigerant and water-glycol fluids, empirical correlations from the open literature were used. A review of the literature found several studies that correlate the heat transfer coefficient for two-phase boiling in corrugated plate heat exchangers [15–24]. The studies that focus on boiling or evaporating heat transfer in plate heat exchangers are tabulated in Table 1, with green and blue shading denoting complete and partial coverage of the parameters in the present study, respectively. The correlations examined in this investigation were based on overlapping parameter ranges.

Though no correlation fully encompassed every flow and thermodynamic parameter in the present study, Huang et al. [17] was the closest: it fully covered heat and mass fluxes ranges, nearly captured all saturation temperatures, was evaluated with R134a, and the plates had a 60° chevron angle. The low mass flux in the Huang et al. [17] investigation caused nucleate boiling to be the dominant heat transfer mechanism and made the flow parameters (i.e. Reynolds number and chevron angle) less significant. The studies by Longo and Gasparella [16,35] encompassed many of the required parameters including mass flux, saturation temperature, and fluid type. Similar to Huang et al. [17], Longo and Gasparella conducted their investigation at low mass fluxes and found that nucleate boiling was the dominant mode of heat transfer in the two-phase region. For example, Longo and Gasparella found that their data compared favorably to the Cooper pool boiling correlation [36], with a mean absolute deviation of 8.2%. The Hsieh et al. [18] investigation encompassed even fewer parameters: heat flux, saturation temperature, and chevron angle. They developed a correlation that combined liquid-phase convective and pool boiling heat transfer. The convective contribution was calculated using the Dittus-Boelter correlation [37] multiplied by an enhancement factor, whereas the pool boiling contribution was calculated by multiplying the Cooper correlation [36] by a suppression factor. The correlation presented by Han et al. [15] was considered due to its dependence on plate geometry, even though it does not encompass many of the parameters of the present investigation. The Nusselt correlation is a function of equivalent Reynolds number, equivalent boiling number, and Prandtl number. Non-dimensional parameters based on the plate geometry are used as the multiplier and Reynolds number exponent.

In the present study, both the refrigerant and water-propylene glycol streams flow as single-phase fluids in the plate frame heat exchanger. The refrigerant experienced a large range of conditions because the fluid entered the heat exchanger as a subcooled liquid and exited as a superheated vapor. For example, the Reynolds numbers ranged from 130 to 3000 with Prandtl numbers between 0.8 and 3.5 throughout the heat exchanger. The water-glycol did not undergo phase change and experienced a smaller range of operational conditions with Reynolds numbers between 180 and 520 and Prandtl numbers from 32 to 34. The conditions were determined from experimental testing of a turbo-compression cooling system test facility which was designed to cool water from 17.2 to 16°C [27]. A review of correlations developed for single-phase heat transfer in plate heat exchangers is summarized in Table 2. The green shading indicates that the correlation fully encompasses both the water-propylene glycol and single-phase refrigerant ranges experimentally tested in this investigation. Blue shading indicates that the parameter partially encompasses both fluids. Purple and red shading indicates that the correlation fully encompasses only the water-propylene glycol or refrigerant, respectively. The single-phase correlations were developed for water or a water-glycol mixture, and no correlations were found for single-phase refrigerant in plate heat exchangers. However, some of the studies cover the Reynolds and Prandtl numbers for the fluids investigated here. As noted in Table 2, the Maslov and Kovalenko [8] correlation was developed for the same chevron angle as the present study, and the valid Reynolds range encompasses both working fluids. None of the investigations that report a Prandtl number range fully encompass the ranges of either fluid in the present study because adding propylene glycol to water dramatically increases the Prandtl number. The Talik et al. [11] investigation does use a water-glycol mixture; however, they utilize a higher glycol concentration than the present study.

Inspection of the literature review highlights a few key points for the present investigation. First, there is currently no boiling correlation for plate heat exchangers that fully encompasses the current test conditions and geometric scale of the current study. Moreover, no study correlates heat transfer coefficient for single-phase refrigerant and there are limited studies which attempt to model a heat exchanger with multiple fluid phase regions. In the present study, an experimentally validated model was developed that spans all three fluid phase regions and several combinations of the presented heat transfer correlations were evaluated. The resulting model could predict heat exchanger performance or plate length using R134a under conditions typical of a turbo-compression cooling system, including low mass flux and heat flux values.

3. HEAT EXCHANGER MODELING APPROACH

The heat exchanger was subdivided to capture the effects of changing fluid transport and thermodynamic properties which impact local pressure drop and heat transfer. Uniform distribution of flow into each channel was assumed for each side. This assumption is justified by comparing the predicted pressure loss though the manifolds relative to the total pressure loss for each fluid. If the manifold pressure loss was a small portion of the total pressure loss for each side, the two fluids were evenly distributed across all the channel sets. The manifold pressure loss was predicted to be 2.2% and 6.3% of the total pressure loss for the refrigerant and water-glycol sides, respectively, which confirms that both fluids were evenly distributed. Each channel set was then divided into a finite number of control volumes. As shown in Figure 1, the two fluids were in a counter flow arrangement. Each control volume is indexed starting with the water-glycol inlet. The index subscript, j, was assigned to each control volume to indicate the outlet refrigerant properties, the inlet water-glycol properties, and the heat transfer of that specific control volume. A sensitivity study was performed resulting in the following number of discrete control volumes for each refrigeration region: 3 for superheated vapor, 12 for two-phase, and 5 for subcooled. Figure 1 also depicts a single control volume including a single refrigerant channel, a single water-glycol channel, and associated plate walls. Heat energy was transferred from the hot water-glycol to the cold refrigerant in both horizontal directions through the plate walls. The heat transfer area for the control volume was the vertical length of the control volume multiplied by the width of the plate, which was the dimension into the page on the right-hand side of Figure 1.

The control volumes can be defined in two ways. The first method was to fix the geometry of the heat exchanger and input the inlet fluid conditions. The outlet fluid conditions were calculated using the heat exchanger model. The second method was to fix the heat duty of the control volume and calculate the required heat transfer area. If the width of the plates was fixed, then the length of the plates would be calculated. While the fixed heat exchanger geometry method was often used in similar studies [34,38], the fixed heat duty method was chosen for the present work because it is more sensitive to a change in heat transfer coefficient. A large change in heat transfer coefficient leads to a large change in predicted length.

The heat duty at each control volume was defined by the refrigerant enthalpy difference between the inlet and outlet of each phase region, multiplied by the refrigerant mass flow rate through a single channel set (150 total sets), divided by the number of control volumes in the phase region. The saturated enthalpies were determined using the saturation conditions at the predicted pressure. The heat duties for control volumes in the subcooled, two-phase, and superheated region were defined by Equation (1) below:

$$q[j] = \left(\frac{i_{\text{in}} - i_{\text{out}}}{CV} \right) \cdot \dot{m}_{\text{r}} \tag{1}$$

In the model, all geometric parameters of the heat exchanger core were held constant except for plate length, which was the dimension in the flow direction. The length term was calculated based on the heat duty calculated in Equation 1 and was used as the primary metric for determining model accuracy. The sum of the lengths for all control volumes was compared to the actual experimental plate length (i.e., measured port to port distance).

Three energy conservation equations were used to relate the heat transfer of the water-glycol to the refrigerant at each control volume, shown in Equations (2) to (4).

$$q = \dot{m}_{\text{r}} \cdot \left(i_{\text{r,out}} - i_{\text{r,in}} \right) \tag{2}$$

$$q = \dot{m}_{\text{g}} \cdot C_{p\,\text{g}} \cdot \left(T_{\text{g,in}} - T_{\text{g,out}} \right) \tag{3}$$

$$q = C_{\min} \cdot \varepsilon \cdot \left(T_{\text{g,in}} - T_{\text{r,in}} \right) \tag{4}$$

$C_{\min}$ in Equation (4) is the minimum heat capacity rate between the refrigerant and water-glycol streams. For the two-phase refrigerant control volumes, the refrigerant specific heat, $C_{p\,\text{r}}$, becomes infinite; therefore, $C_{\min}$ was determined using Equation (5).

$$C_{\min} = C_{p\,\mathrm{g}} \cdot \dot{M}_{\mathrm{g}} \tag{5}$$

The next step was to incorporate the geometric parameters and heat transfer coefficients using a thermal resistance network. At each control volume the resistance network included three thermal resistances in-series: a water-glycol convective resistance, a wall conductive resistance, and a refrigerant convective resistance. The convective resistances were determined using Equation (6) and the wall conduction resistance was determined using Equation (7).

$$R_{\mathrm{conv}} = [h \cdot A_p]^{-1} \tag{6}$$

$$R_{\mathrm{wall}} = \frac{\delta_{\mathrm{wall}}}{k_{\mathrm{wall}} \cdot A_{\mathrm{wall}}} \tag{7}$$

The convective heat transfer coefficient, h, in Equation (6) was calculated using empirical correlations found in literature. Fouling resistances are commonly included in heat exchanger resistance networks to account for deposit build up, which restricts the transfer of heat. For this investigation, the fouling resistances were neglected because of the limited operating hours of the experimental heat exchanger.

The resistance network was then used to quantify an overall conductance (*UA*) and calculate the number of transfer units (*NTU*) at each control volume, as shown in Equations (8) and (9).

$$UA = \left(R_{\mathrm{r}} + R_{\mathrm{wall}} + R_{\mathrm{g}}\right)^{-1} \tag{8}$$

$$NTU = \frac{UA}{C_{\min}} \tag{9}$$

The effectiveness-NTU relationship for counter flow heat exchangers, shown in Equation (10), connected the thermodynamic and heat transfer portions of the model by relating the thermal resistance network to the effectiveness of each control volume.

$$NTU = \frac{1}{C_r - 1} \ln\left(\frac{\varepsilon - 1}{\varepsilon \cdot C_r - 1}\right) \tag{10}$$

In Equation (10), C_r was the ratio of C_{min} over C_{max}. With the heat exchanger model completed, several of the heat transfer correlations discussed in Section 2 were compared to experimental data to determine the combinations of single-phase and boiling correlations that resulted in the highest model accuracy.

4. EXPERIMENTAL SETUP AND DATA COLLECTION

The present study collected data by using a preexisting turbo-compression cooling system (TCCS), which is a thermally activated cooling system designed to generate cooling from low grade waste heat [27]. As shown in Figure 2, the system operates as an organic Rankine cycle (ORC) directly coupled to a vapor compression cycle (VCC). The liquid-coupled evaporator in the VCC was the primary focus of the present investigation.

The VCC evaporator in the TCCS test facility was a plate frame heat exchanger comprised of 300 corrugated stainless steel plates separated by rubber gaskets. The space between two adjacent plates forms a channel for fluid flow. These channels alternate between the water-glycol hot side fluid, and the R134a cold side working fluid. The water-glycol was a 70% water, 30% propylene glycol by volume mixture. During experimentation, R134a entered the heat exchanger as a subcooled liquid, evaporated, and exited as a superheated vapor. The corrugated plates were sheets of stamped steel as shown in Figure 3. The plates include fluid inlet and outlet ports, a diffuser and reducer with guide vanes, and a corrugated heat transfer surface with a chevron pattern. The chevrons are used to generate turbulence and increase local fluid velocity to increase the heat transfer coefficient [39]. The plate frame heat exchanger used in this study had a double V chevron pattern with a 60° angle from the vertical, was 0.432 m wide, and was 1.2 m long. The evaporator was tested over a range of refrigerant mass fluxes between 5.8 kg m^{-2} s^{-1} and 6.8 kg

m^{-2} s^{-1}, heat fluxes between 2 kW m^{-2} and 2.8 kW m^{-2}, and at saturation temperatures between 10°C and 15°C. Data collection was performed with water-glycol inlet temperatures between 15°C and 25°C.

Figure 4 displays an instrumented process flow diagram of the evaporator in the test facility. The evaporator was instrumented with T-type thermocouples and Ashcroft type G1 pressure transducers at the inlet and outlet of the heat exchanger. The refrigerant mass flow rate was also measured just before the expansion valve using an inline Coriolis mass flow meter. During all tested conditions for the TCCS operation, the refrigerant entered the evaporator subcooled. Therefore, the inlet temperature and pressure were sufficient to determine inlet enthalpy. Due to inaccuracies of the water-glycol volume flow measurements, the water-glycol mass flow rate was determined using an energy balance calculation across the evaporator.

An important testing consideration was to ensure that the water-glycol and refrigerant temperatures did not converge. During testing, it was common for the temperature of the outlet refrigerant to converge to the inlet temperature of the water-glycol because of the desired operational conditions and limitations of the test facility. When this occurred, it was impossible to determine the location where the refrigerant reached its maximum temperature. Figure 5 represents possible temperature profiles for a temperature converging counter flow heat exchanger. The solid line represents the water-glycol temperature versus location and the dashed lines represent possible refrigerant temperature profiles where the position of the maximum temperature was unknown. The unknown refrigerant temperature profile indicates that one boundary condition was missing and the model cannot be validated. Experiments were conducted such that the temperature differences at each end of the heat exchanger were above 0.5°C. This was achieved by increasing the refrigerant mass flow rate to a point where the outlet refrigerant was minimally superheated.

A Wilson plot experiment was used to determine the water-glycol side heat transfer coefficient. The experiment varied the water-glycol flow rate over a range of data points, while maintaining constant refrigerant side conditions. The refrigerant side inlet and outlet conditions, as well as the refrigerant mass flow rate were held as constant as possible to collect all data points. The minimal variability allowed for the assumption that the refrigerant thermal resistance was constant across the experiment. The constant thermal resistance assumption was also made by Yanik and Webb [40] when performing similar experiments. If the refrigerant convective resistance and wall conductive resistance remain constant across all of the collected points, then the water-glycol convective resistance was the only resistance that will change in the overall thermal resistance calculation as a function of the water-glycol flow rate. The water-glycol flow rate was then reduced to a velocity term and the overall thermal resistance of the heat exchanger was plotted as a function of the water-glycol velocity to the power of negative N for all the points collected. A linear regression was then determined for the data. The value of N was varied to maximize the R^2 value of the regression. The regression was then set equivalent to the Equation (11).

$$R_{\mathrm{ov}} = \frac{1}{C_2 \cdot A_{\mathrm{g}}} \cdot \frac{1}{\bar{V}_{\mathrm{g}}^{N}} + C_1 \tag{11}$$

The regression was used to calculate coefficients C_1 and C_2. The sum of the refrigerant and wall resistances was equal to C_1, shown in Equation (12).

$$C_1 = R_{\mathrm{r}} + R_{\mathrm{wall}} \tag{12}$$

C_2 was used to determine the water-glycol heat transfer coefficient for each of the data points collected by using Equation (13).

$$h_g = C_2 \cdot \bar{V}_g^{N} \tag{13}$$

The water-glycol heat transfer coefficient was then compared to the coefficients calculated for the same data points using the single-phase correlations discussed in Section 2.

The uncertainty of the experimentally calculated values used in the model validation effort was critical to determine the relevance of the effort. The three parameters of interest for the uncertainty propagation study were: the overall heat transfer rate, the water-glycol side heat transfer coefficient, and the water-glycol mass flow rate. To determine the uncertainty of the three parameters, the built in uncertainty propagation function in Engineering Equation Solver [41] was used. The function uses the standard method of error propagation in Equation (14).

$$S_y = \sqrt{\sum_{\mathrm{i}=1}^{\mathrm{n}} \left(\frac{\partial y}{\partial x_{\mathrm{i}}} \right)^2 S_{x_{\mathrm{i}}}^2} \tag{14}$$

In this equation, S_{y} represents the variable of interest and S_{x} represents each variable used in the calculation of S_{y}.

The uncertainties associated with the instruments used in data collection, shown in Table 3, and the actual data collected values were used as inputs to the uncertainty analysis. These inputs were propagated through the model to calculate the uncertainty of the three experimentally determined parameters of interest. For example, to calculate the overall heat transfer rate, the measured refrigerant temperature and pressure were used to determine the enthalpies at the heat exchanger inlet and outlet. The uncertainty of the measured values was propagated through the enthalpy calculations. The inlet and outlet enthalpies, along with the measured refrigerant mass flow rate were used to calculate the total heat transfer rate using Equation (15).

$$q = \dot{m}_{\mathrm{r}} \cdot \left(i_{\mathrm{r,out}} - i_{\mathrm{r,in}} \right) \tag{15}$$

The three parameters and associated uncertainties were used as inputs into the right-hand side of Equation (14) to determine the uncertainty of the experimentally calculated heat transfer rate. A similar process was performed to determine the uncertainty of the water-glycol mass flow rate calculation, and water-glycol heat transfer coefficient calculated from the Wilson plot experiment.

Table 4 presents the results of the uncertainty study for the data collected. The uncertainty of the heat transfer rate was small: between 0.54% and 0.55%. The water-glycol mass flow rate uncertainty was more significant: between 34% and 141%. The lower uncertainty occurred when the water-glycol mass flow rate was small, which corresponded to a larger temperature change between the inlet and outlet. A smaller temperature difference resulted in a large uncertainty in the mass flow calculation. The high uncertainty in the mass flow produce very high uncertainty in determining the water-glycol heat transfer coefficient in the Wilson plot experiment and the correlation calculated coefficient. The effect of this uncertainty on the correlation calculated coefficients is further discussed in the results section. The third parameter of interest in the uncertainty study was the Wilson plot experiment calculated water-glycol heat transfer coefficient. This uncertainty ranged from 17% to 66%, where the higher uncertainty occurred when the water-glycol mass flow rate was the highest.

5. RESULTS AND DISCUSSION

The heat transfer model was validated with experimental data from a TCCS. The validated range of refrigerant mass fluxes from 5.8 to 6.8 kg m^{-2} s^{-1}, heat fluxes from 2 to 2.8 kW m^{-2}, and saturation temperatures from 10 to 15°C. The model was first validated for the water-glycol side heat transfer coefficient using a Wilson plot experiment. Several steady state data points were collected, and the overall thermal resistance was plotted as a function of the water-glycol velocity to the negative N power, as shown in Figure 6. N was varied until the linear regression achieved an R^2 value greater than 97.5%. The resulting N value was equal to 0.5. The water-glycol heat transfer coefficient was then calculated from the regression equation and compared to seven single-phase heat transfer correlations: Muley [12], Thonon et al. [7], Maslov and Kovalenko [8], Rosenblad and Kullendroff [9], Emerson [10], Talik et al. [11], and Kumar [14] as presented in Section 2. Table 5 shows the mean absolute error (MAE) of the model predicted heat transfer coefficient compared to the Wilson plot generated coefficients. Muley [12] resulted in the lowest MAE, equal to 0.136%. As discussed in the previous section, the uncertainty in the water-glycol heat transfer coefficient calculated from the Wilson Plot was high, reaching 66%, and was considered when comparing correlations. Figure 7 shows the water-glycol heat transfer coefficient as a function of water glycol velocity for each of the correlations tested as well as the four Wilson plot points with associated error bars. Though some of the correlations, particularly Rosenblad and Kullendroff [9], and Maslov and Kovalenko [8], are within the upper end of three of the error bars, the correlations have significant inaccuracies at low flow rates. The coefficient at the lowest water-glycol velocity is the most significant to accurately predicting the trend because this point has the least uncertainty. The Muley correlation [12] followed the experimental trend to the highest level of accuracy and therefore refrigerant-side model validation was performed using the Muley correlation to represent the water-glycol side heat transfer coefficient.

With the wall conduction resistance calculated from known parameters, the refrigerant side thermal resistance was the only remaining variable to be experimentally validated in the heat transfer model. Three single-phase heat transfer correlations and four boiling heat transfer correlations were tested in a matrix to determine the most accurate combination for the studied range of conditions. The correlations were used to predict the plate length of the heat exchanger core which was compared to the actual plate length of the heat exchanger under test. The three single-phase correlations tested were Thonon [7], Maslov and Kovalenko [8], and Rosenblad and Kullendroff [9]. The single-phase heat transfer coefficient had a minor impact on the predicted plate length relative to the boiling heat transfer coefficient because less than 1% of the heat transfer was in the single-phase region. A change in the single-phase correlation resulted in about a 0.2 m change in the predicted plate length. The boiling correlations discussed used the Thonon single-phase correlation [7] for representative result values because it was a part of the combination resulting in the lowest MAE.

The four two-phase heat transfer correlations, discussed in Section 2, tested for accuracy within the model were Huang et al. [17], Cooper [28], Hsieh et al. [18], and Han et al. [15]. The correlations were used to predict the required plate length of the core for given inlet and outlet conditions. Of the four boiling correlations selected, Huang et al. [17] was the only correlation that under-predicted the heat exchanger plate length. When used to represent the two-phase boiling region, the Huang et al. correlation [17] predicted the plate length on average to be 0.735 m, 38.7% lower than the actual length. The remaining three boiling correlations all over-predicted the plate length. The predicted length for all correlation combinations within the plate frame heat exchanger is shown in Figure 8 (a). The black bar at 1.2 m represents actual heat exchanger length. Similarly, Figure 8 (b) shows the predicted core length error compared to the actual plate length. The correlations over predict the plate length due to an under prediction of the heat transfer coefficient, and not due to temperature "pinching". As shown in Table 6, for all data collected the effectiveness values of each of the three phase regions were between 0.2 and 0.7. In addition, Figure 9 shows that two-phase region dominates the UA requirement of the heat exchanger. The different colors represent separate data points collected. The three refrigerant phase regions are separated by the vertical black bars. Most of the overall heat exchanger UA was in the two-phase refrigerant region. This means that the large predicted plate lengths were not caused by small differences in high effectiveness values resulting from the uncertainty of the heat transfer rate calculation. If the heat exchanger had high effectiveness values in the two-phase regions, and the uncertainty of the heat transfer rate allowed the effectiveness to vary between 0.95 and 0.99, this would cause a large difference in predicted plate length. However, at lower effectiveness values, the low heat transfer rate uncertainty does not cause a significant variability in the predicted length term.

The Han et al. correlation [15] underpredicted the heat transfer coefficient due to extrapolation errors associated with using the correlation outside of the developed heat and mass flux ranges. The Cooper correlation [36] was less accurate because the correlation was developed for pool boiling. Though Longo and Gasparella [16,35] credit the use of their correlation in plate evaporators at low mass fluxes, the correlation does not capture any effects of flow boiling. The Hsieh et al. correlation [18] showed a strong sensitivity in the heat transfer coefficient from an increase in heat flux. The correlation validated heat flux range is 10 kW m^{-2} to 30 kW m^{-2}, five to ten times the range seen in the present investigation. The lower heat fluxes underpredicted heat transfer coefficients. The Huang et al. correlation [17] predicted the plate length most accurately because it was used within almost all of the developed parameter ranges. However, the heat exchanger in this study operated at low refrigerant mass fluxes and the plate length was not accurately represented by any of the empirical correlations tested.

One inaccuracy with the Huang et al. [17], Hsieh et al. [18], and Cooper [36] correlations was that, like many other boiling correlations, the heat transfer was a function of heat flux, which made accurate modeling challenging because the length term and heat transfer coefficient were interconnected multiple times in the model. Thus, the model was solved through iteration when calculating the plate length and caused numerical instability while solving for the heat transfer performance. To mitigate this, the length term in the heat flux calculations was fixed to 0.060 m for each control volume, which was the length between inlet and outlet ports divided by the number of control volumes. The length term used to calculate the plate area in the thermal resistance network, Equations (6) and (7), remained to be calculated. This reduced computational complexity at the expense of some accuracy because the true heat flux was not used. By fixing the lengths in the heat flux calculation, the average predicted length for the Huang et al. [17] correlations changed to 0.742 m, as shown in Figure 10 (a). This was a slightly lower than 1% increase in the calculated plate length and the correlation still under predicted the actual plate length. With a fixed control volume length value of 0.060 m, the predictive length using the Cooper correlation [36] reduced to 1.86 m and 54.7% MAE relative to the data, and the Hsieh et al. correlation [18] reduced to 1.22 m and 5.5% MAE, as shown in Figure 10. Hsieh et al. [18] was more accurate than the Cooper correlation [36] likely because of the incorporation of the convective component with the Cooper pool boiling correlation. Furthermore, for all the single-phase correlations combined with the Hsieh et al. correlation [18], only one data point fell outside of ±25% error, which occurred when the Muley correlation [12] was used for the single-phase region and resulted in 29% error.

The combination of single-phase and two-phase correlations that resulted in the smallest MAE was the Thonon [7] and Hsieh et al. [18] correlations when a fixed length term was used for heat flux calculations and resulted in a MAE equal to 5.5%. These two correlations should be used to represent the refrigerant side heat transfer, along with the Muley correlation [12] to represent the water-glycol side heat transfer, in future plate heat exchanger models with similar operating conditions.

6. CONCLUSIONS

The objective of the present study was to develop and validate a heat exchanger model for a plate frame evaporator which included three fluid regions: subcooled liquid, two-phase boiling, and superheated vapor. A vapor compression cycle in a turbo-compression cooling system test facility was used to collect data for model validation. The experimental mass flux, heat flux, and saturation temperatures of the refrigerant within the evaporator of the cooling cycle ranged from 5.8 to 6.8 kg m^{-2} s^{-1}, 2 to 2.8 kW m^{-2}, and 10 to 15°C, respectively. The model used empirical correlations found in the literature to determine the required plate length of the heat exchanger core. Wilson plot experiments were conducted to determine the experimental water-glycol side heat transfer coefficients. When compared to the Wilson plot calculated coefficients, the Muley correlation [12] was found to be the most accurate with a MAE of 0.14%. Four boiling and three single-phase heat transfer correlations were tested in a matrix to determine the refrigerant side heat transfer within all fluid phase regions. The correlations without modification were unable to accurately predict the heat transfer performance of the heat exchanger operating at low mass flux ranges. The combinations that used the Huang et al. [17] boiling correlation were the most accurate, and with the Maslov and Kovalenko [8] single-phase correlation the MAE was -32.3%. When the correlations used a fixed control volume length in the heat flux calculation, the most accurate combination (5.5% MAE) was the Hsieh et al. [18] boiling, and Thonon [7] single-phase correlations.

Future work will continue data collection to further validate the model through a wider range of operating conditions and heat exchanger geometries. The current data set is small and limits the model to a narrow range of validated conditions. Future experiments aim to reduce model error by collecting data in manners which reduce the uncertainty of the water-glycol heat transfer coefficient calculation. New correlations for single and two-phase flow through plate heat exchangers could also be tested to determine if a set is better suited for the evaporating heat exchanger than the correlations tested in the present study. In addition, the authors envision further work that will produce discretized models for condensing plate frame heat exchangers, with experimental validation of the condensing models.

ACKNOWLEDGMENTS

The authors would like to acknowledge the Department of Energy Advanced Research Project Agency-Energy (ARPA-e) for their support under contract DE-AR0000574, for the funding for the Turbo-Compression Cooling System test facility which allowed for the this study to be conducted. The authors would also like to acknowledge the support form Barber-Nichols Inc. and the State of Colorado OEDIT program for funding associated with this work.

REFERENCES

[1] S. Bendapudi, J. E. Braun, and E. A. Groll, “A comparison of moving-boundary and finite-volume formulations for transients in centrifugal chillers,” *Int. J. Refrig.*, 2008, doi: 10.1016/j.ijrefrig.2008.03.006.

[2] M. W. Browne and P. K. Bansal, “Heat transfer characteristics of boiling phenomenon in flooded refrigerant evaporators,” *Applied Thermal Engineering*. 1999, doi: 10.1016/S1359-4311(98)00056-8.

[3] M. W. Browne and P. K. Bansal, “An elemental NTU-ε model for vapour-compression liquid chillers,” *Int. J. Refrig.*, 2001, doi: 10.1016/S0140-7007(00)00091-8.

[4] E. Torrella, J. Navarro-Esbrí, and R. Cabello, “Boiling heat-transfer coefficient variation for R407C inside horizontal tubes of a refrigerating vapour-compression plant’s shell-and-tube evaporator,” *Appl. Energy*, 2006, doi: 10.1016/j.apenergy.2005.01.010.

[5] J. Navarro-Esbrí *et al.*, “Shell-and-tube evaporator model performance with different two-phase flow heat transfer correlations. Experimental analysis using R134a and R1234yf,” *Appl. Therm. Eng.*, 2014, doi: 10.1016/j.applthermaleng.2013.09.009.

[6] R. K. Shah, “Heat Exchangers,” in *Encyclopedia of Energy Technology and the Eviroment*, A. Bisco and S. G. Boots, Eds. New York: John Wiley & Sons, 1994, pp. 1651–1670.

[7] B. Thonon, R. Vidil, and C. Marvillet, “Recent Research and Developments in Plate Heat Exchangers,” *J. Enhanc. Heat Transf.*, vol. 2, no. 1–2, pp. 149–155, 1995, doi: 10.1615/JEnhHeatTransf.v2.i1-2.160.

[8] A. Maslov and L. Kovalenko, “Hydraulic resistance and heat transfer in plate heat exchangers,” *Molochnaya Promyshlenflost*, vol. 10, pp. 20–22, 1972.

[9] G. Rosenblad and A. Kullendorff, “Estimating heat transfer rates from mass transfer studies on plate heat exchanger surfaces,” *Wärme- und Stoffübertragung*, 1975, doi: 10.1007/BF01681560.

[10] W. H. Emerson, “The Thermal and Hydrodynamic Performance of a plateheat Exchanger: II A DeLaval Exchanger,” *Natl. Eng. Lab.*, 1995.

[11] A. C. Talik, L. S. Fletcher, N. K. Anand, and L. W. Swanson, “Heat transfer and pressure drop characteristics of a plate heat exchanger using a propylene glycol–water mixture as the working fluid,” 1995.

[12] A. Muley, “Heat Transfer and Pressure Drop in Plate Heat Exchangers,” University of Cincinnati, 1997.

[13] A. Muley and R. M. Manglik, “Experimental Study of Turbulent Flow Heat Transfer and Pressure Drop in a Plate Heat Exchanger With Chevron Plates,” *J. Heat Transfer*, 1999, doi: 10.1115/1.2825923.

[14] S. Kumar, S. D. Heister, X. F. Xu, J. R. Salvador, and G. P. Meisner, “Thermoelectric Generators for Automotive Waste Heat Recovery Systems Part I: Numerical Modeling and Baseline Model Analysis,” *J. Electron. Mater.*, vol. 42, no. 4, pp. 665–674, 2013, doi: 10.1007/s11664-013-2471-9.

[15] D. H. Han, K. J. Lee, and Y. H. Kim, “Experiments on the characteristics of evaporation of R410A in brazed plate heat exchangers with different geometric configurations,” *Appl. Therm. Eng.*, 2003, doi: 10.1016/S1359-4311(03)00061-9.

[16] G. A. Longo and A. Gasparella, “Refrigerant R134a vaporisation heat transfer and

pressure drop inside a small brazed plate heat exchanger," *Int. J. Refrig.*, 2007, doi: 10.1016/j.ijrefrig.2006.11.011.
[17] J. Huang, T. J. Sheer, and M. Bailey-Mcewan, "Heat transfer and pressure drop in plate heat exchanger refrigerant evaporators," 2012, doi: 10.1016/j.ijrefrig.2011.11.002.
[18] Y. Y. Hsieh, L. J. Chiang, and T. F. Lin, "Subcooled flow boiling heat transfer of R-134a and the associated bubble characteristics in a vertical plate heat exchanger," *Int. J. Heat Mass Transf.*, 2002, doi: 10.1016/S0017-9310(01)00294-0.
[19] Y.-Y. Yan and T.-F. Lin, "Evaporation Heat Transfer and Pressure Drop of Refrigerant R-134a in a Plate Heat Exchanger," *J. Heat Transfer*, 1999, doi: 10.1115/1.2825924.
[20] G. N. Danilova, "Correlation of Boiling Heat Transfer Data for Freons," *Heat Transf. Res.*, vol. 2, no. 2, pp. 73–78, 1970.
[21] D. Sterner and B. Sunden, "Performance of plate heat exchangers for evaporation of ammonia," 2006, doi: 10.1080/01457630600559611.
[22] S. C. Palmer, W. V. Payne, and P. a Domanski, "Evaporation and Condensation Heat Transfer Performance of Flammable Refrigerants in a Brazed Plate Heat Exchanger," *NIST Interagency/Internal Rep.*, 2000.
[23] Z. H. Ayub, "Plate heat exchanger literature survey and new heat transfer and pressure drop correlations for refrigerant evaporators," *Heat Transf. Eng.*, 2003, doi: 10.1080/01457630304056.
[24] E. Lee, H. Kang, and Y. Kim, "Flow boiling heat transfer and pressure drop of water in a plate heat exchanger with corrugated channels at low mass flux conditions," *Int. J. Heat Mass Transf.*, 2014, doi: 10.1016/j.ijheatmasstransfer.2014.05.019.
[25] F.A.S. Mota, E.P. Carvalho, and M.A.S.S. Ravagnani, "Modeling and Design of Plate Heat Exchanger," Heat Transfer Studies and Applications, Salim Newaz Kazi, IntechOpen, 2015, DOI: 10.5772/60885.
[26] R. A. Peixoto and C. W. Bullard, "A Design Model For Capillary Tube Suction Line Heat Exchangers," *ACRC TR-53*, 1994.
[27] S. D. Garland, J. Noal, and T. M. Bandhauer, "Experimentally validated modeling of a turbo-compression cooling system for power plant waste heat recovery," *Energy*, vol. 156, pp. 32–44, 2018.
[28] R. Eldeeb, V. Aute, and R. Radermacher, "A survey of correlations for heat transfer and pressure drop for evaporation and condensation in plate heat exchangers," *Int. J. Refrig.*, vol. 65, pp. 12-26, 2016.
[29] R. L. Amalfi, F. Vakili-Farahani, and J. R. Thome, "Flow boiling and frictional pressure gradients in plate heat exchangers. Part 1: Review and experimental database," *Int. J. Refrig.*, vol. 61, pp. 166-184, 2016.
[30] R. L. Amalfi, F. Vakili-Farahani, and J. R. Thome, "Flow boiling and frictional pressure gradients in plate heat exchangers. Part 2: Comparison of literature methods to database and new prediction methods," *Int. J. Refrig.*, vol. 61, pp. 184-203, 2016.
[31] T. Lv, B. Zheng, W. Li, and Z. Ayub, "A Modified Correlation for Flow Boiling Heat Transfer in Plate Heat Exchangers," *J. of Therm. Sci. and Eng. Appl.*, vol. 12, pp. 1-12, 2020.
[32] G. A. Longo, S. Mancin, G. Righetti, C. Zilio, "A new model for refrigerant boiling inside Brazed Plate Heat Exchangers (BPHE)," *Int. J. of Heat and Mass Transf.,* vol. 91, pp. 144-149, 2015.
[33] H. Lee, S. Li, Y. Hwang, R. Radermacher, H. Chun, "Experimental investigations on flow

boiling heat transfer in plate heat exchanger at low mass flux condition," *Appl. Therm. Eng.*, vol 61, pp. 408-415, 2013.
[34] H. Jeong, J. Oh, and H. Lee, "Experimental investigation of performance of plate heat exchanger as organic Rankine cycle evaporator," *Int. J. Heat Mass Transf.*, vol. 159, 2020, doi: 10.1016/j.ijheatmasstransfer.2020.120158.
[35] G. A. Longo and A. Gasparella, "Heat transfer and pressure drop during HFC refrigerant vaporisation inside a brazed plate heat exchanger," *Int. J. Heat Mass Transf.*, 2007, doi: 10.1016/j.ijheatmasstransfer.2007.07.001.
[36] M. G. Cooper, "Heat Flow Rates in Saturated Nucleate Pool Boiling-A Wide-Ranging Examination Using Reduced Properties," *Adv. Heat Transf.*, 1984, doi: 10.1016/S0065-2717(08)70205-3.
[37] F. W. Dittus and L. M. K. Boelter, "Heat transfer in automobile radiators of the tubular type," *Int. Commun. Heat Mass Transf.*, vol. 12, no. 1, pp. 3–22, 1985, doi: 10.1016/0735-1933(85)90003-X.
[38] E. Y. Gurbuz, A. Sozen, H. I. Variyenli, A. Khanlari, A. D. Tuncer, "A comparative study on utilizing hybrid-type nanofluid in plate heat exchangers with different number of plates," J. of the Brazilian Soc. of Mech. Sci. and Eng., 2020, doi: 10.1007/s40430-020-02601-1
[39] D. C. Lee, D. Kim, S. Park, J. Lim, and Y. Kim, "Evaporation heat transfer coefficient and pressure drop of R-1233zd(E) in a brazed plate heat exchanger," *Appl. Therm. Eng.*, 2018, doi: 10.1016/j.applthermaleng.2017.11.088.
[40] M. K. Yanik and R. L. Webb, "Prediction of two-phase heat transfer in a 4-pass evaporator bundle using single tube experimental data," *Appl. Therm. Eng.*, 2004, doi: 10.1016/j.applthermaleng.2003.10.023.
[41] S. A. Klein and F. Alvarado, "Engineering Equation Solver," *F-Chart Software*. 2002.
[42] D. Chisholm and A. S. Wanniarachchi, "Plate heat exchangers: plate selection and arrangement," 1990.
[43] T. S. Khan, M. S. Khan, M. C. Chyu, and Z. H. Ayub, "Experimental investigation of single phase convective heat transfer coefficient in a corrugated plate heat exchanger for multiple plate configurations," *Appl. Therm. Eng.*, 2010, doi: 10.1016/j.applthermaleng.2010.01.021.
[44] M. A. Hessami, "Laminar to turbulent flow transition in cross-corrugated-plate cavities," 1998.

List of figures:

List of Tables:

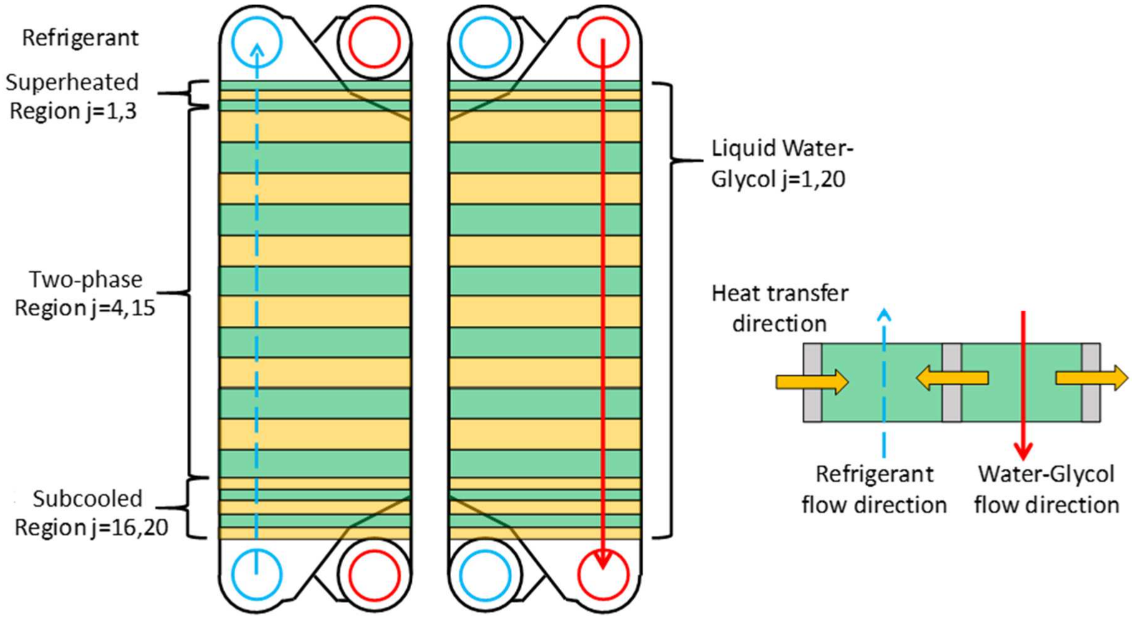

Figure 1. Plate frame heat exchanger discretization.

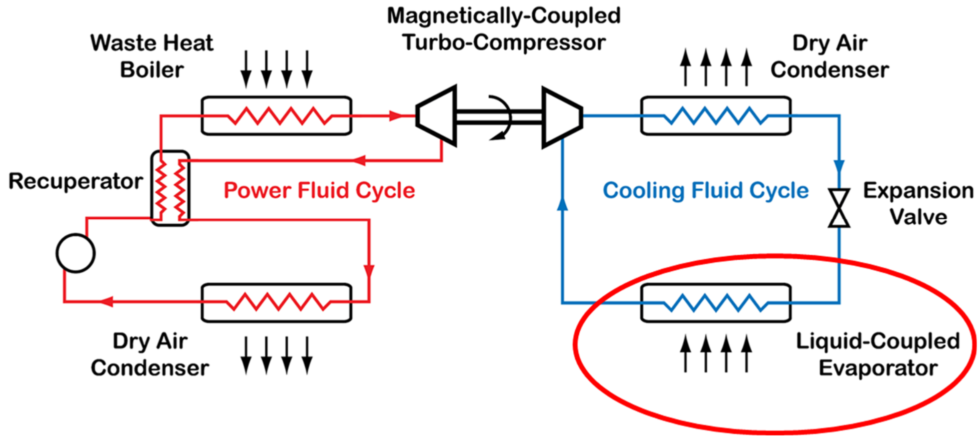

Figure 2. Simplified diagram of the turbo-compression cooling system test facility.

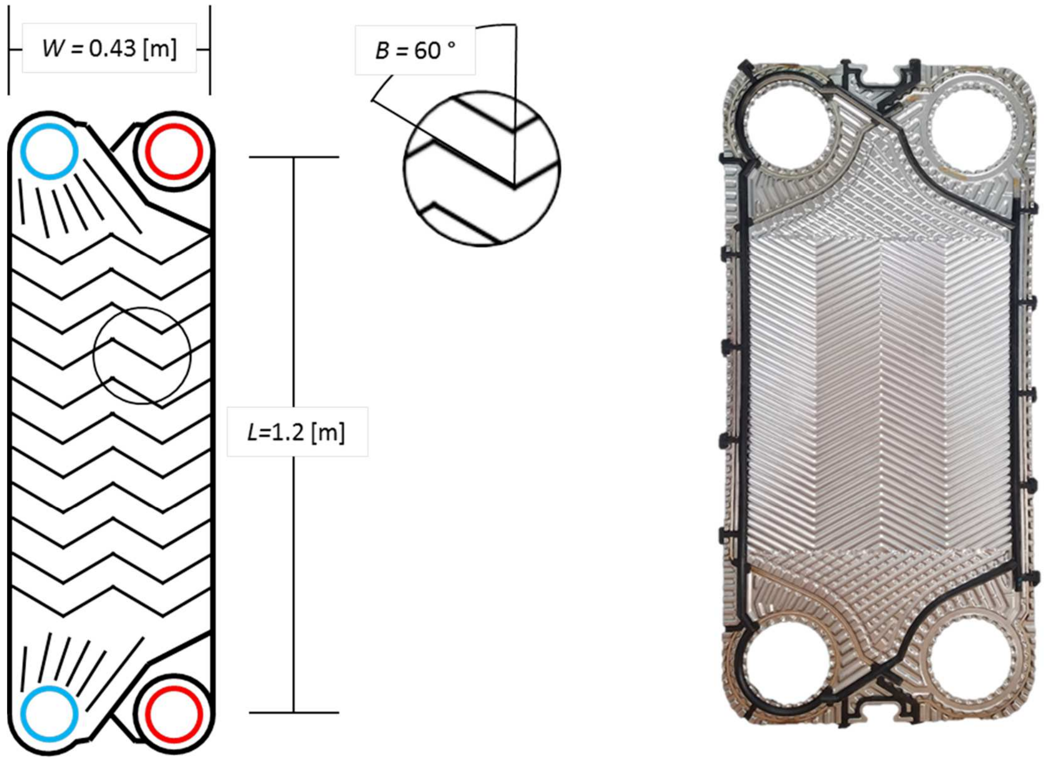

Figure 3. Geometry overview of the plate frame heat exchanger investigated in the current study.

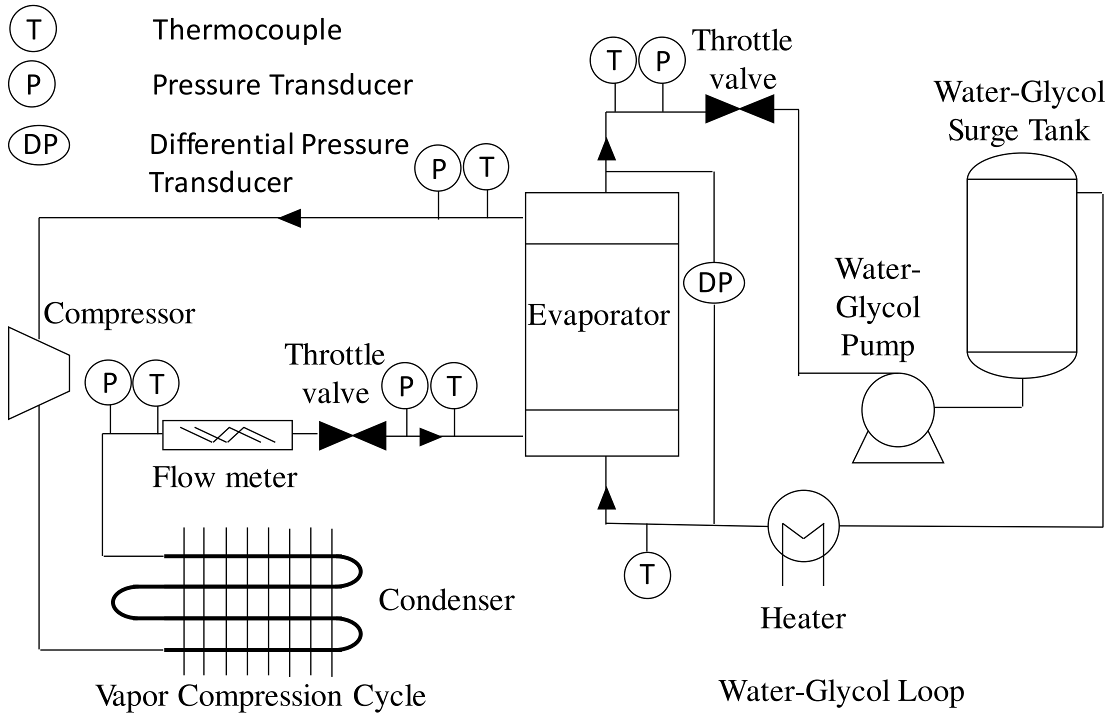

Figure 4. Piping and instrumentation diagram of the evaporator test facility.

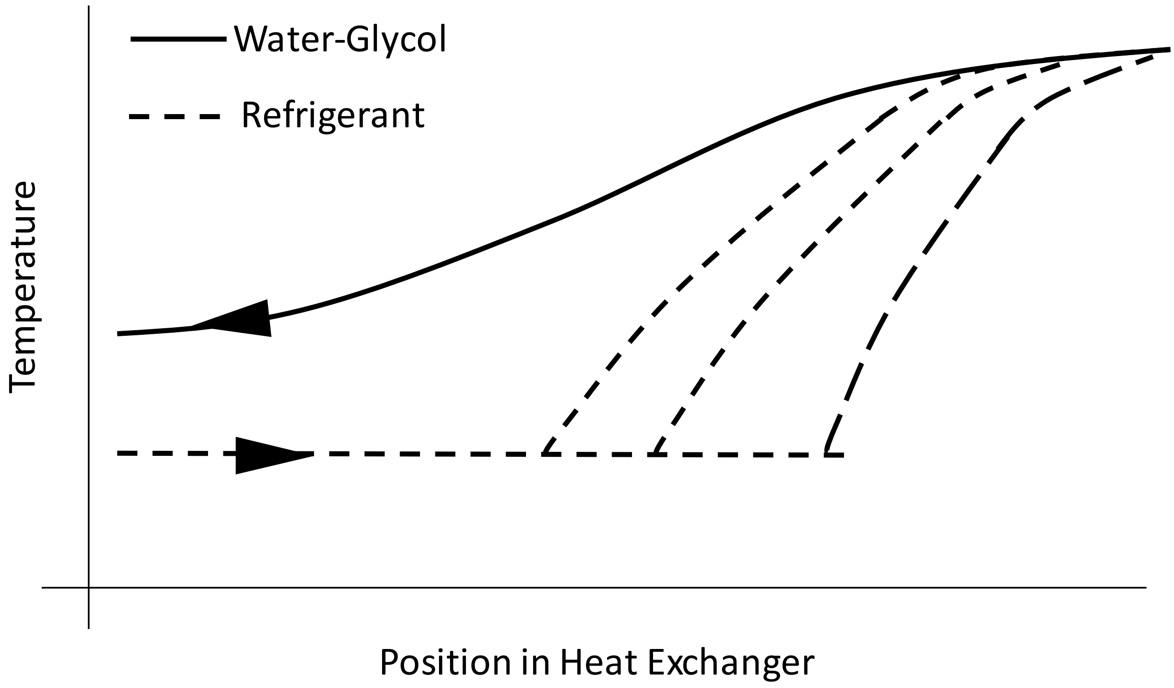

Figure 5. Counter flow temperature profile of an oversized evaporative heat exchanger where the temperature of the refrigerant and water-glycol converge.

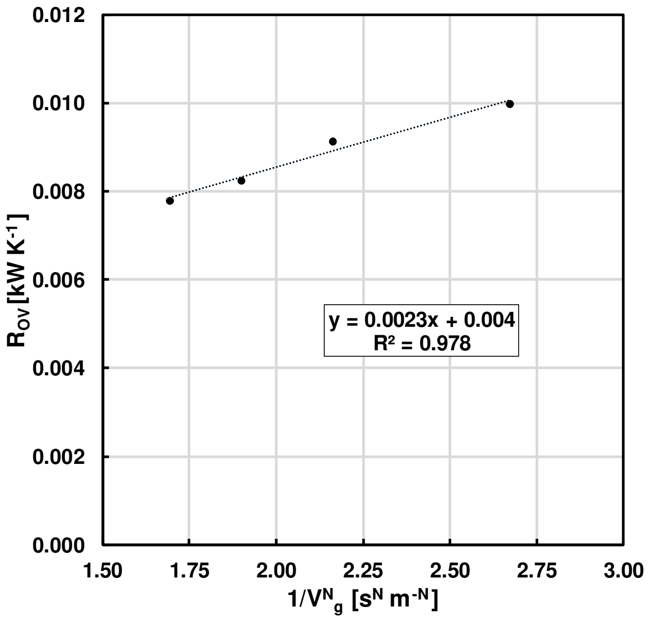

Figure 6. The experimental results from the Wilson plot studies for the water-glycol heat transfer coefficient.

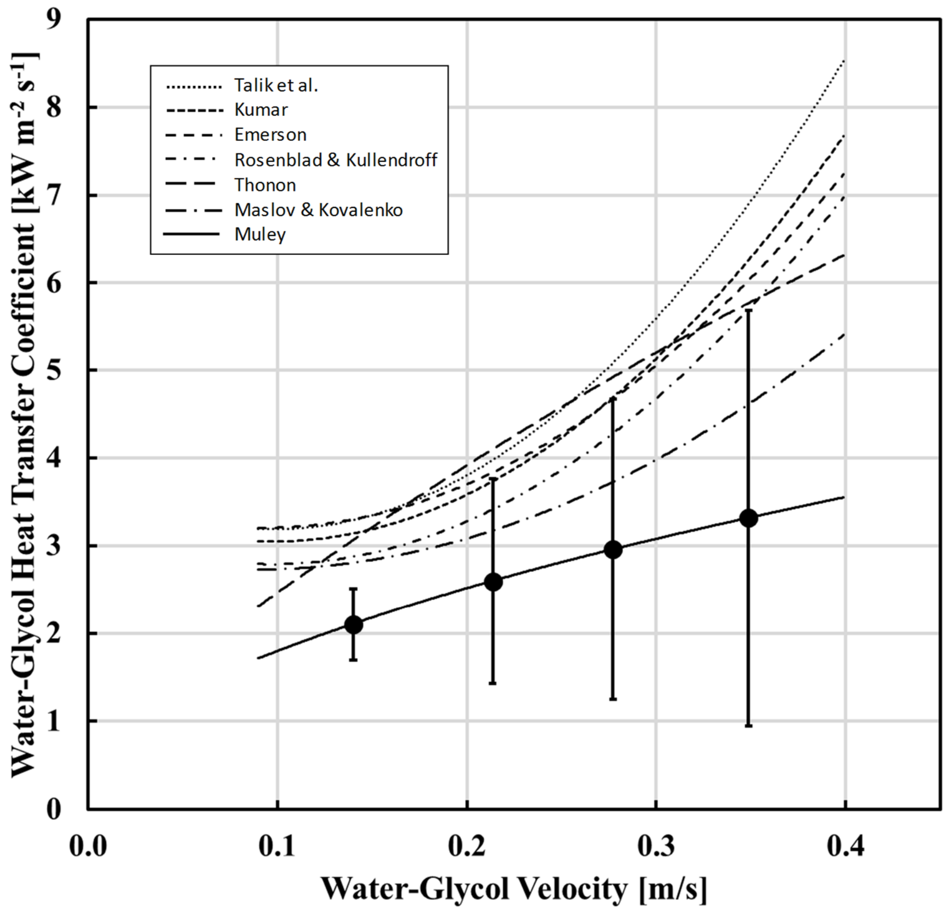

Figure 7. Comparison of the Wilson plot calculated water-glycol heat transfer coefficient to the coefficients calculate from correlations in the open literature.

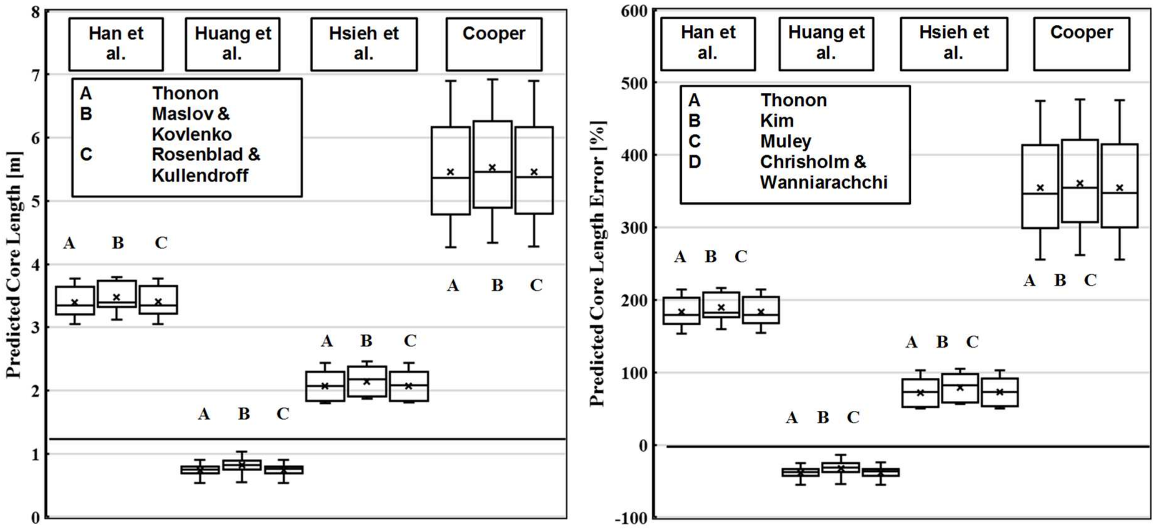

(a) (b)

Figure 8. The results of the predicted core length based on various refrigerant heat transfer correlations.

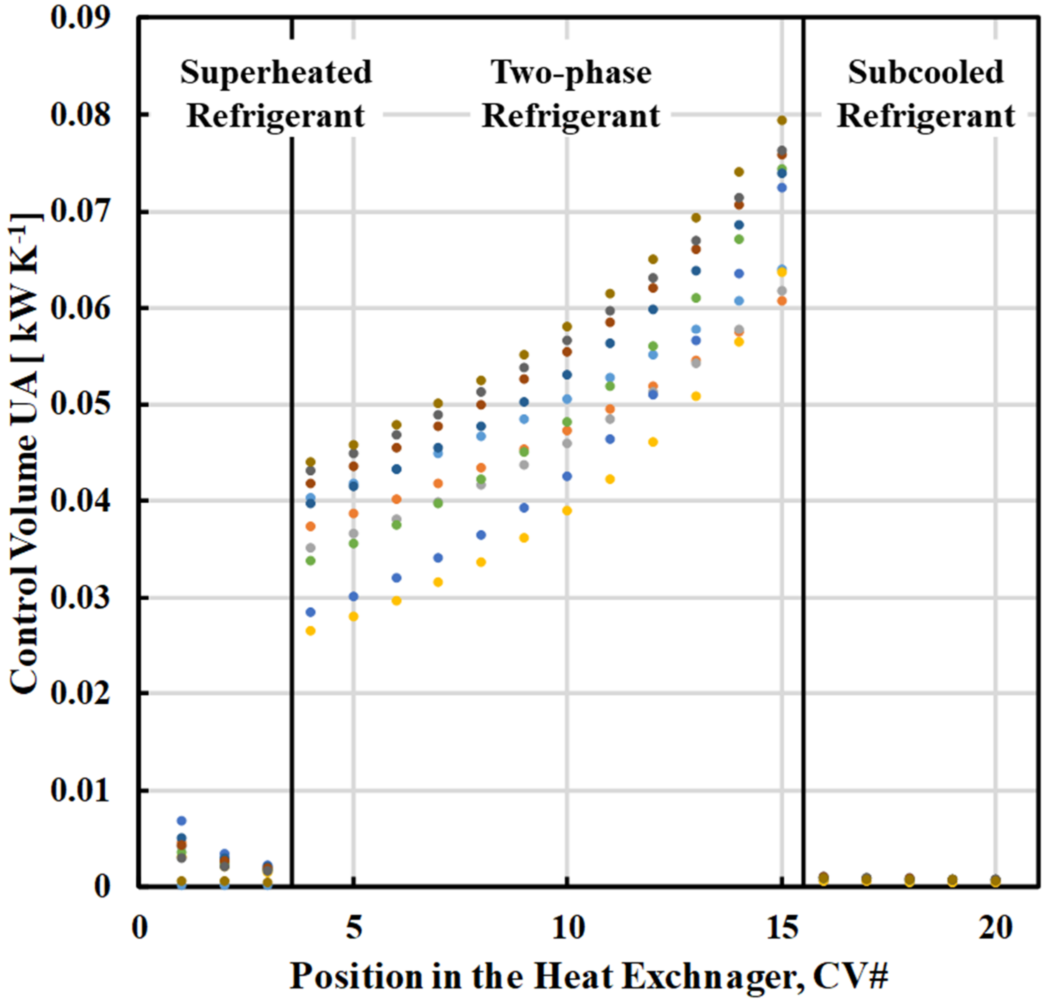

Figure 9. Distribution of UA along the heat exchanger control volumes for a single plate set.

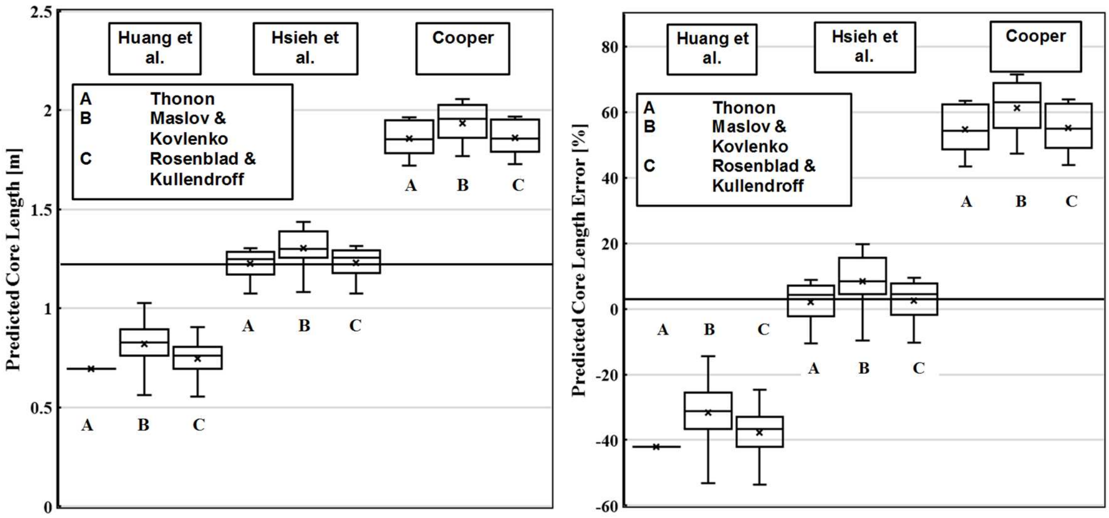

(a) **(b)**

Figure 10. Results of the refrigerant heat transfer coefficient correlations tested with a fixed length in the heat flux term.

Table 1. Review of two-phase boiling heat transfer and pressure drop correlations.

Name	Working Fluid	# of Channels	Heat Transfer	Pressure Drop	Chevron Angle	mass flux		heat flux		T_{sat}		L	w	dh
	-	-			degree	kg m^{-2} s^{-1}		kW m^{-2}		°C		mm	mm	mm
Present Study	**R134a**	**150**			**60**	**5.8**	**6.8**	**2**	**2.8**	**10**	**15**	**1200**	**430**	**5.1**
Han et al. [15]	R22 / R410	3	X	X	20,35,45	13	34	2.5	8.5	5	15			
Hsieh and Lin [18]	R410	2	X	X	60	50	125	2	37	10	30	450	120	6.6
Huang et al.[17]	R134a / R507a / R12 / Ammonia	23	X	X	28,44,60	5.6	30.3	1.9	7	5	13	519	180	3.5
Lee et al. [33]	R1233zd(E)	Unknown	X	X	60	5.5	27	6	49	105	105	357	103	4.4
Longo Gasparella [16] [35]	R410	9	X		65	4	50	3	21	5	20	278	72	3.2
	R134a / R410 / R245fa	9	X		65	4	50	3	21	5	20	278	72	3.2
Yan and Lin [19]	R134a	2	X	X	60	55	70	11	15	31	31	450	120	5.9

Table 2. Review of single-phase heat transfer coefficient correlations.

Name	Working Fluid	Heat Transfer	Pressure Drop	Chevron Angle	Re		Pr		dh
	-			degree	-		-		mm
Present Study	**R134a**			**60**	**130**	**3000**	**0.8**	**3.5**	**5.1**
Present Study	**Water-Glycol**			**60**	**180**	**520**	**32**	**34**	**5.1**
Chisholm and Wanniarachchi [42]	Water	X		30-80	1000	40000	5	5	
Muely and Manglik [13]		X	X	30,45,60	600	10000	2	6	5.08
Khan [43]		X		30,45,60	500	2500	3.5	6.5	3.9
Thonon [7]	water	X	X	30,45,60,75	60	2415			
Muely [12]		X	X	30-60	30	400			
Maslov and Kovalenko [8]	Water	X		60	50	20000			
Talik et al. [11]	Water-Glycol	X	X	60	10	720	70	450	4.65
	Water	X	X		14500	11460	2.5	50	4.65
Hessami [44]		X		45,60	200	1800			11
Emerson [10]	Water	X			10	25			
		X			40	1000			
Longo and Gasparella [16]	Water	X		65	200	1200	5	10	
Kumar [14]	Water	X		60	20	400			
Rosenblad and Kullendorff [9]	Water	X		60	60	2415			4

Table 3. Reported uncertainty values for the instrumentation in the evaporator test facility.

Instrument Type	Range	Accuracy
Thermocouple	All	0.6°C
Diff. Pressure Transducer	0-15 PSI	1.5% FS
	0-35 PSI	1.5% FS
Pressure Transducer	0-200 PSI	0.25% FS
Mass Flow Meter	0-7.5 kg s^{-1}	0.15% MV

Table 4. The results of the uncertainty propagation on the relevant model inputs.

Total heat transfer rate [kW]		Water-Glycol mass flow rate [kg s^{-1}]		Water-Glycol heat transfer coefficient [kW m^{-2} k^{-1}]	
Value	Uncertainty	Value	Uncertainty	Value	Uncertainty
185	1.016	66.61	94.03	3.602	2.369
186.4	1.016	55.29	60.35	3.282	1.71
187.9	1.023	43.93	36.01	2.925	1.166
186.3	1.013	22.16	8.749	2.078	0.4073
215.7	1.173	22.12	7.499	2.076	0.35
213.3	1.17	31	15.11		
215.5	1.183	44.71	32.04		
215.2	1.182	49.36	39.63		
214.4	1.18	52.42	45.3		
211.3	1.17	53.81	48.78		

Table 5. Single-phase heat transfer coefficient correlation predictions compared to Wilson plot experiment generated coefficients.

Wilson Plot	Thonon [7]	Muley [12]	Talik et al. [11]	Kumar [14]	Maslov & Kovalenko [8]	Emerson [10]	Rosenblad & Kullendroff [9]
3.629	6.51	3.62	7.650	6.886	4.935	6.544	6.264
3.317	5.77	3.32	6.719	6.104	4.520	5.888	5.558
2.957	4.92	2.96	5.663	5.202	4.032	5.124	4.743
2.596	4.10	2.60	3.405	3.231	2.871	3.388	2.958
2.101	3.06	2.11	3.464	3.290	2.896	3.435	3.011
%MAE	64.7	0.14	80.183	66.149	31.408	65.023	51.565

Table 6. Effectiveness values for the subcooled, two-phase, and superheated regions of the evaporator for the data.

ε: Subcooled	ε: Two-phase	ε: Superheated
0.22	0.24	0.05
0.24	0.27	0.62
0.24	0.32	0.59
0.20	0.46	0.49
0.26	0.49	0.70
0.27	0.43	0.50
0.30	0.35	0.60
0.30	0.33	0.55
0.29	0.32	0.42
0.27	0.32	0.11